Available online at www.sciencedirect.com
ScienceDirect
Trans. Nonferrous Met. Soc. China 24(2014) 2713−2722
Transactions of Nonferrous Metals Society of China
www.tnmsc.cn

# Electrochemical corrosion behavior of arc sprayed Al−Zn−Si−RE coatings on mild steel in 3.5% NaCl solution

Qiong JIANG, Qiang MIAO, Fei TONG, Yi XU, Bei-lei REN, Zhi-mei LIU, Zheng-jun YAO

College of Material Science and Technology, Nanjing University of Aeronautics and Astronautics, Nanjing 211100, China

Received 2 July 2013; accepted 13 December 2013

**Abstract:** Al−Zn−Si−RE coating with high Al content was deposited on mild steel by arc spraying. The electrochemical behavior of Al−Zn−Si−RE coating in 3.5 % NaCl solution was systematically studied by potentiodynamic polarization, corrosion potential ($\varphi_{corr}$) and electrochemical impedance spectroscopy techniques (EIS). The impedance data were fitted to appropriate equivalent circuits to explain the different electrochemical processes occurring at the electrode-electrolyte interface. The results indicate that Al−Zn−Si−RE coating reveals the similar polarization behavior as Zn−15Al coating. The coating has no passive region in the anodic polarization, but far lower corrosion current and much higher corrosion potential. Al−Zn−Si−RE coating provides effective sacrificial protection for steel substrate and the sacrificial anodic protection plays dominant role during the immersion process. In addition, the $\varphi_{corr}$ evolution and EIS plots indicate that the corrosion process can be divided into five stages: pitting−dissolution−redeposition, activation corrosion, cathodic protection, physical barriers and the coating failure.

**Key words:** Al−Zn−Si−RE coating; corrosion potential; corrosion behavior; polarization plots; electrochemical impedance spectroscopy

## 1 Introduction

Zn−Al sacrificial coatings by flame and wire-arc spray have been widely used for the long-term corrosion protection of steel by combining the great galvanic protection of Zn with the satisfactory erosion resistance of Al [1−4]. In these coatings, the presence of micro porosity and/or oxide content is no longer be a problem, since the coating acts as sacrificial anode with respect to the substrate and protects the latter at its own expense by itself corroding or dissolving preferentially. ORLANDO et al [2,5] found that the thermally sprayed Zn−Al coating exhibited excellent corrosion resistance, even without the use of sealant, providing excellent galvanic protection to the substrate. Therefore, there has been recently growing interest in exploring the corrosion behavior of Zn−Al coating, which offers valuable insights into the improvement of corrosion resistance.

Several studies showed that the addition of micro alloying elements such as Si, Mg, Mn and rare earth (RE) elements into Zn−Al alloy can produce substantial improvements in corrosion resistance and abrasion resistance [6−9]. RE elements, primarily La and Ce, can also improve the wettability and fluidity of molten melts, purify melts and refine the cast microstructure of metals which will not appreciably affect their resistance to corrosion [9−11]. In addition, precious researchers [12−15] found that the corrosion resistance of Zn−Al alloy coating could be dramatically improved by increasing the Al content. Therefore, the research on multicomponent Zn−Al-based alloy wires with high Al content has evoked great interest during the last few years. FENG et al [16] developed series of Al−Zn−Si−RE alloy solid wires. However, there was no systematic studies on the corrosion behavior and mechanism of Al−Zn−Si−RE coating.

The corrosion behavior of thermally sprayed Zn and Zn-based coatings has been studied and reported [12,17], however, little research has been conducted on the

**Foundation item:** Project (CXLX12_0149) supported by Funding of Jiangsu Innovation Program for Graduate Education, China; Project (BA2011029) supported by Special Fund of Transformation of Sci-tech Achievements of Jiangsu Province, China; Project (BY2011101) supported by the Creative Fund of Combination of Industry, Academia and Research of Jiangsu Province, China—Prospective Joint Research Project; Project (kfjj120217) supported by Open Funds of NUAA Innovation Base (Laboratory) for Graduate Students

**Corresponding author:** Qiang MIAO; Tel: +86-25-52112904; Fax: +86-25-52112626; E-mail: miaoqiang@nuaa.edu.cn

DOI: 10.1016/S1003-6326(14)63402-6

corrosion mechanism of the Al−Zn-based coatings with high Al content up to 50%. Electrochemical evaluation techniques, such as potentiodynamic polarization and electrochemical impedance spectroscopy (EIS), have been shown in corrosion research to be efficient and convincing tools for analyzing the corrosion behavior of metals [18,19]. In this study, potentiodynamic polarization, open circuit potential (OCP) and electrochemical impedance spectroscopy (EIS) techniques were carried out to study the corrosion behavior of the Al−Zn−Si−RE coating with high Al content systematically in quiescent 3.5% NaCl solution.

## 2 Experimental

### 2.1 Coating material

Zn−15Al and Al−Zn−Si−RE alloy wires (2 mm in diameter), were used as wire materials, and their compositions are listed in Table 1. Cold-rolled Q235 steel plate with dimensions of 5 cm × 7 cm × 0.3 cm was used as substrate. The substrates were degreased ultrasonically in acetone and grit blasted with corundum at the pressure of about 550 Pa just prior to spraying, to remove any contamination from the surface and generate roughened surface that promotes coating adhesion. Compressed air was used to remove any residue from the grit blasting. The coatings were deposited with HAS-02 high velocity arc spraying gun and system CDM AS3000 at normal temperature. Spray conditions are summarized as follows: spraying voltage of 30−32 V, spraying current of 120−140 A, air pressure of 0.65 MPa and spraying distance of 60−120 mm. The samples were cut into small sections (2 cm × 2 cm) in order to allow corrosion tests whose cut edges were sealed by epoxy.

**Table 1** Elements content of alloy wires (mass fraction, %)

| Alloy | Al | Si | RE | Zn |
|---|---|---|---|---|
| Al−Zn−Si−RE | 50−55 | 0.2−3 | 0.02−2 | Bal. |
| Zn−15Al | 10−15 | − | − | 85−90 |

At least two rare-earth elements selected from the group consisting of La, Ce, Pr and Nd

### 2.2 Corrosion tests

In order to have better understanding of the corrosion behavior of the coatings, the corrosion potential ($\varphi_{corr}$) evolution curves, potentiodynamic polarization curves and electrochemical impedance spectroscopy (EIS) were carried out using CHI660d electrochemical working station. All tests were conducted in naturally aerated 3.5% NaCl (mass fraction) solution at room temperature. These experiments were carried out several times and were reproducible. Traditional three-electrode cell was used, with 4 $cm^2$ platinum sheet as counter electrode, saturated calomel electrode (SCE) immersed in saturated KCl solution as the reference electrode and test specimen with exposed area of 1.0 $cm^2$ as the working electrode. The coating thickness was around 60 μm.

All potentials in this study were reported with respect to saturated calomel reference electrode (SCE). Potentiodynamic polarization studies were carried out in the potential range from −0.30 V to 0.60 V versus corrosion potential at sweep rate of 2 mV/s. All potentiodynamic polarization experiments were conducted after stabilization of free corrosion potentials. The EIS measurements were measured at $\varphi_{corr}$ over a frequency range from 10 mHz to 100 kHz. The EIS data were analyzed and fitted to appropriate equivalent circuits using the ZSimpWin software. The quality of fitting to equivalent circuit was judged firstly by the Chi-square value ($\chi^2$, i.e., the sum of the square of the differences between theoretical and experimental points) and secondly by limiting the relative error in the value of each element in the equivalent circuit to 5% [20,21]. The equivalent circuits were chosen based on the number of time constants and the quality of fits [22,23].

## 3 Results

### 3.1 Potentiodynamic polarization

Figure 1 shows the potentiodynamic polarization curves of Al−Zn−Si−RE coating, Zn−15Al coating and bare steel in 3.5% NaCl solution during initial stage of immersion. The electrochemical parameters such as corrosion potential ($\varphi_{corr}$), corrosion current density ($J_{corr}$), polarization resistance ($R_p$), anodic Tafel slope ($\beta_a$) and cathodic Tafel ($\beta_c$) are listed in Table 2.

According to Fig. 1, the Al−Zn−Si−RE coating and Zn−15Al coating show $\varphi_{corr}$ values of −0.965 V and −1.112 V, respectively. These values are approximately 300 mV more negative than that of steel substrate (−0.643 V), which indicates that both the coatings can

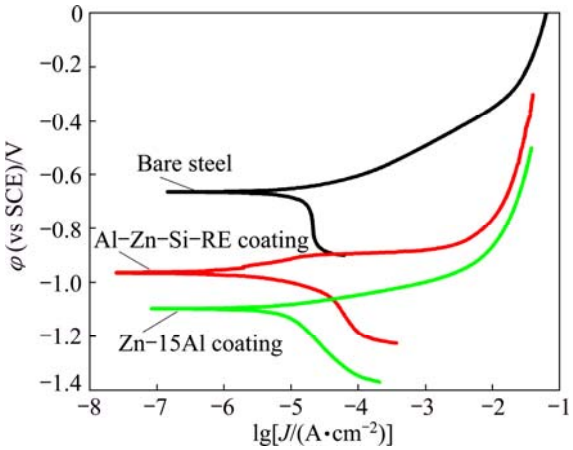


**Fig. 1** Potentiodynamic polarization curves of Al−Zn−Si−RE coating, Zn−15Al coating and bare steel in 3.5% NaCl solution

**Table 2** Electrochemical parameters obtained from polarization curves during initial stage of immersion

| System | $\varphi_{corr}$(vs SCE)/V | $R_p$/(Ω·cm$^2$) | $J_{corr}$/(μA·cm$^{-2}$) | $\beta_c$/(mV·dec$^{-1}$) | $\beta_a$/(mV·dec$^{-1}$) |
|---|---|---|---|---|---|
| Steel substrate | −0.643 | 1446.5 | 28.14 | 102.5 | 1080 |
| Al−Zn−Si−RE coating | −0.965 | 1218.5 | 36.54 | 287.8 | 159.3 |
| Zn−15Al coating | −1.112 | 464.4 | 40.41 | 168.9 | 58.0 |

provide sufficient driving force for cathodic protection to substrate [24,25]. In addition, polarization curve of Al−Zn−Si−RE coating appears obvious activation platform above the $\varphi_{corr}$, at which the current density increases sharply, indicating the initiation of pitting corrosion [26]. Therefore, Al−Zn−Si−RE coating shows good surface activation as the sacrificial anode materials [8,27]. As can be seen from Table 2, Al−Zn−Si−RE coatings exhibit cathodic Tafel slopes significantly higher than anodic Tafel slopes, which indicates that the electrochemical corrosion behaviors of the coating are dominated by the cathode reaction [28]. It is not beneficial to forming stable anode passivation layers on the surface, so the Al−Zn−Si−RE coating exhibits active dissolution characteristics [29]. It is well known that the corrosion current is an important parameter commonly used to assess the kinetics of corrosion reactions, and it is almost directly proportional to the corrosion rate [30,31]. Al−Zn−Si−RE coating shows very similar polarization behavior as that of Zn−15Al coating, and has no passive region in the anodic polarization region. A less negative value of $\varphi_{corr}$ and lower value of $J_{corr}$ for Al−Zn−Si−RE coating clearly confirm the better corrosion resistance than Zn−15Al coating. These findings agree well with the other published results [9,32] that the increase of Al content and the addition of Si can improve the corrosion resistance of the Zn−Al coating in NaCl solution.

### 3.2 Measurements of $\varphi_{corr}$

Corrosion potential is referred to as mixed potential that reflects combined outcome of all electrochemical reactions occurring at the electrode-solution interface [33,34]. The variation of the corrosion potential with the immersion time can be employed to study the electrochemical corrosion processes, qualitatively evaluate the corrosion protection performance of coatings and judge coating failure. The $\varphi_{corr}$ evolution with time allows to follow the electrochemical activity of the Zn and Zn−Al coatings, and the electrochemical processes proceeding in such systems are usually assumed to be the oxidation of zinc or aluminum particles ($Zn \rightarrow Zn^{2+}+2e$ or $Al \rightarrow Al^{3+}+3e$) and the reduction of dissolved oxygen ($O_2+2H_2O+4e \rightarrow 4OH^-$) in electrolyte [35,36]. It was reported that the evolution of $\varphi_{corr}$ was closely related to the variation of the ratio of electroactive areas (Zn−Al alloy/steel) [35,37].

It is believed that the cathodic protection (CP) duration by Zn or Zn−Al coatings to substrate steel can be defined as the duration period when the $\varphi_{corr}$ value of the coating/substrate system remains lower than −0.85 V [35,36,38]. Figure 2 shows the variation of corrosion potential with respect to testing time for Al−Zn−Si−RE coating in 3.5% NaCl solution, indicating that the corrosion process goes through five stages as follows.

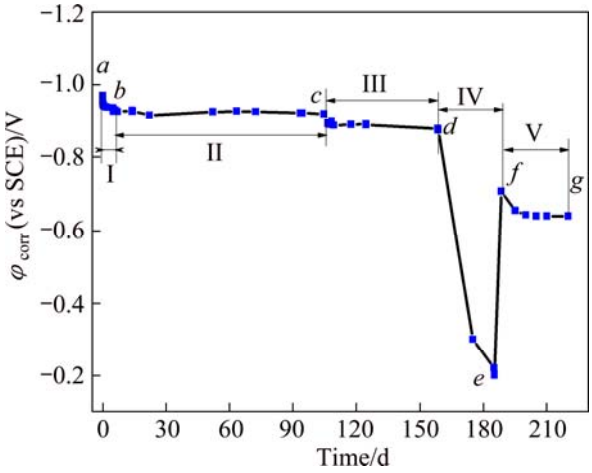


**Fig. 2** Evolution of corrosion potential $\varphi_{corr}$ with immersion time for Al−Zn−Si−RE coating

Period I: At the beginning of immersion, the $\varphi_{corr}$ shifts quickly toward noble potential values.

Periods II and III: A long-term relative stabilization is observed, indicating that sacrificial anodic action plays the dominant position during the whole immersion process with long CP durations. The potential continues to shift positively at much slower rate with immersion time. This phenomenon is similar to that reported in Refs. [35−38].

In the former three stages, the active region decreases and the protection provided by the corrosion products layer is enhanced progressively with increasing immersion time. As a result, the dynamic equilibrium between the dissolution of metal particles and the formation of corrosion products is established and then the potential remains relatively constant. According to Refs. [35,37], the positive shift in the values of $\varphi_{corr}$ is generally ascribed to the reduction of the electroactive surface area of Al−Zn particles, which also means a decrease in the intensity of cathodic protection.

Period IV: After 175 d immersion, $\varphi_{corr}$ suddenly increases, and it continually rises to maximum value of −0.20 V after 185 d immersion. This phenomenon is generally associated with the coverage isolation of internal active Al−Zn−Si−RE particles by the zinc aluminum corrosion products in coating [35,37]. At this stage, the barrier properties caused by compact corrosion product layer hold the dominant position, but they have very short duration. Later the potential value quickly shifts negatively.

Period V: At the end of immersion, corrosion potential tends to become constant and approaches −0.64 V, which is the corrosion potential of the un-coated mild carbon steel in 3.5% NaCl solution. The corrosion scale is destroyed, the corrosion media comes into direct contact with substrate and the substrate is corroded [38].

### 3.3 EIS characteristics

The Nyquist and Bode plots corresponding to the Al−Zn−Si−RE coating at different immersion time exposed in 3.5% NaCl solution are shown in Fig. 3. The measured EIS spectra are generally the average impedance of coating-substrate system. According to Fig. 3, the Nyquist diagrams exhibit multi-time constants during periods of immersion, and even new time constant corresponding to diffusive resistance occurs in the latter stage. It is clearly observed that the shape of Nyquist plots changes greatly in the low frequency ranges. The reason is that the low-frequency region in EIS plots usually conveys important information on the electrode-controlled process in conjunction with the contribution from localized defects to the overall impedance [33,34,39−41]. The electrochemical corrosion processes of Al−Zn−Si−RE coating with time can be clearly divided into six stages based on the shape of the impedance curve.

During the initial stage of immersion, Nyquist plots were characterized by three time constants, namely, small capacitive loop at high frequencies, big capacitive loop at medium frequencies and inductive loop at low frequencies (see Fig. 3(a)). The high-frequency behavior can be ascribed to electrolyte penetration including water uptake and salt intrusion [34]. The medium-frequency semicircle is typical associated with the charge transfer of the corrosion process and the double layer behavior at the coating-electrolyte interface [42,43]. The presence of low-frequency inductive loop may be attributed to the relaxation processes obtained by adsorbed species (such as chloride and the intermediate products formed during the pitting process) [26,44−46]. The moderate pitting is favorable factor for the activation alloys [26]. Polarization resistance drops dramatically as soon as pit nucleation occurs on the electrode surface, and accordingly the low frequency inductive behavior appears [47].

The diameter of the capacitive loops in the Nyquist plane represents the polarization resistance of the test specimens, and the larger capacitive loop means the lower corrosion rate [48,49]. As seen in Figs. 3(a) and (b), the magnitude of the capacitive loop represented by the semicircle diameter increased with time indicating substantial decrease in the corrosion rate. This behavior is attributed to the deposition of corrosion products in the defects, which deters the adsorption of chloride and the redeposition of $Zn^{2+}$ and $Al^{3+}$ ions onto the coating surface [27].

As shown in Figs. 3(c) and (d), the Nyquist plots of EIS data during the second stage are very similar in shape. The Nyquist plots present two capacitive loops, and the inductance behavior has disappeared. The small high-frequency capacitive loop is correlated with the contact resistance between the alloy particles in the coating, and the large capacitive loop in low frequency region is attributed to the electrochemical behavior of the activation area on the electrode surface. Regarding the immersion time, it seems that the diameter of the semicircles later is smaller than the former, indicating the increase of rates of electrochemical reactions. This may be because more and more metal particles participate in the dissolution reaction due to the electrolyte uptake by the coating with the immersion time. At this stage, the aggressive species (such as O, $Cl^-$ and $H_2O$) diffuse progressively through the defects and permeate onto the surface of metal particles, which contributes to the activation corrosion. The Al−Zn−Si−RE coating still exhibits good barrier property against corrosion media, because the corrosion products deposited in the defects provides favorable self-healing behavior. This indicates that the corrosion process is still controlled by uniform activation corrosion, and the electron transfer can become the rate-controlling step of the electrochemical process [50].

The EIS spectra in the third corrosion period (see Figs. 3(e) and (f)) present similar characteristics, except that the radius of capacitive loop at low frequency decreases with time. Compared to the former stage, the high-frequency semicircle becomes more apparent. The corrosion products gradually clog the pores between the metal particles with time, and thereupon result in the increase of the coating resistance.

The evolution of EIS diagrams at the fourth stage is shown in Figs. 3(g) and (h). It can be seen that the Nyquist diagram consists of two depressed semicircles. The evolution of time exhibits no significant change in the diameter of the high-frequency semicircle associated with the impedance of the coating itself, but a progressive increase in the diameter of the low-frequency semicircle attributes to the electrochemical reactions at

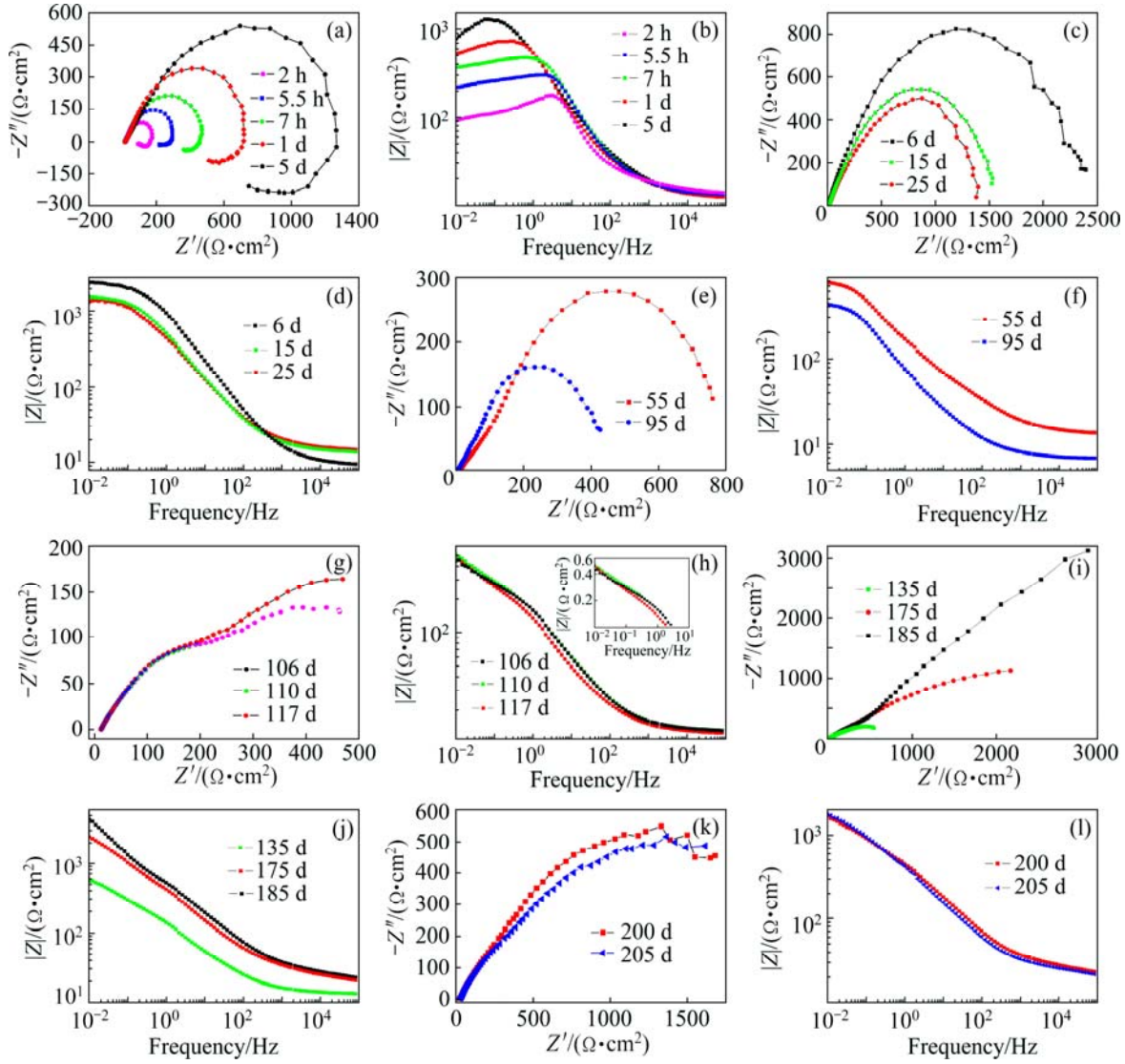


**Fig. 3** Nyquist plots and corresponding Bode plots of Al−Zn−Si−Si coating for different immersion time in 3.5% NaCl solution: (a, b) Initial stage; (c,d) Second stage; (e,f) Third stage; (g, h) Fourth stage; (i, j) Fifth stage; (k, l) Sixth stage

the coating/substrate interface. On the one hand, the corrosion products accumulate inside the defects between the alloy particles and hinder further penetration of the electrolyte, which results in an increase of the coating resistance. On the other hand, the corrosion product layer formed on the surface of metal particles covers the surface electroactive area of internal alloy particles [51], and the number of metal particles participating in the reaction are greatly decreased. These factors decrease the dissolution of alloy particles in the coating and contribute to the cathodic protection durability.

At the fifth stage of immersion, as shown in Figs. 3(i) and (j), the capacitive loops at low frequencies are all incomplete, and the dimensions of the depressed semicircles increase with immersion time. The presence of large capacitive loop at the low frequencies may denote the formation of protective corrosion scale on the substrate surface [52]. After 185 d of immersion, the Nyquist plot shows a high frequency semicircle and a tail at the medium and low frequencies with slope of inclination of nearly 1. The Bode plot shows limited capacitive characteristic but frequency-independent impedance in the low-frequency range [53]. This type of characteristics provides evidence that the diffusion controlled process with mass transfer occurs along the corrosion product layer [54,55]. At this time, the corrosion products accumulate within the coating and act as barrier, and thus the mass transfer becomes the major rate-controlling step in this process [56,57].

At the sixth stage (Figs. 3(k) and (l)), the shape of spectra with respect to time is similar, and there is a substantial decrease in the diameter of the low-frequency semicircle. Corrosion potential at this time is gradually close to the bare steel potential. At this stage, the coating presents poor barrier against the diffusion of species.

Therefore, the coating exhibits rather poor resistance to $Cl^-$ attack and corrosion occurs on the substrate surface, which is consistent with Period V of the $\varphi_{corr}$−$t$ curve.

According to Fig. 3, the impedance value of the low frequency varies with immersion time. Since the information from low frequency in Bode diagram mainly reflects the impedance of the coating (combination of capacitive and resistive behaviors), the impedance at the lowest frequency, $|Z|_{f\to 0}$, can be used to evaluate the corrosion protection abilities of the coating systems to some extent [58]. The higher value of $|Z|_{f\to 0}$ implies lower corrosion rate of the materials [59]. The modulus at 0.01 Hz, $|Z|_{0.01Hz}$, is also shown as a function of immersion time in Fig. 4.

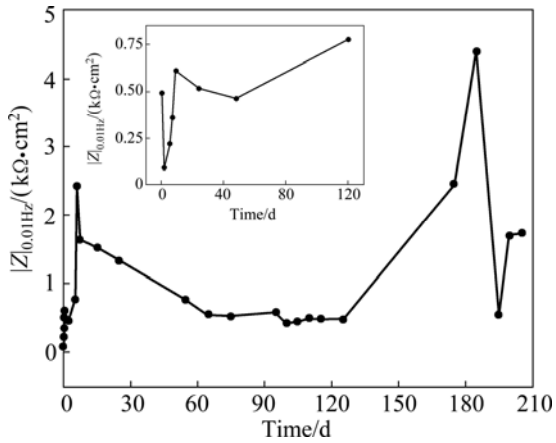


**Fig. 4** Evolution of low frequency modulus $|Z|_{0.01Hz}$ with immersion time for Al−Zn−Si−RE coating

As can be seen in Fig. 4, the value of $|Z|_{0.01Hz}$ has a sudden decrease in the beginning due to the occurrence of pitting corrosion and then a sharp increase due to the deposition of corrosion products. There is a decrease in the value of $|Z|_{0.01Hz}$ after 5 d of immersion which can be adequately explained by the activation of the alloy particles and the progression of the electrolyte into the coating [35]. The $|Z|_{0.01Hz}$ value gradually increases with time after 120 d immersion because of the isolation of the alloy particles by the corrosion products in the coating [35,37]. After immersion for 185 d, the corrosion resistance of the coating is greatly improved by enhancing the value of $|Z|_{0.01Hz}$ by one order of magnitude. However, this process exhibits extremely short duration. After 195 d immersion, a significant decrease in the value of $|Z|_{0.01Hz}$ is observed, revealing that the corrosion resistance of coating decreases with immersion time.

## 4 Discussion

The impedance data of Al−Zn−Si−RE coating was fitted with suitable equivalent circuit models to explain the different electrochemical processes occurring at the electrode-electrolyte interface. Nyquist plots and the fitting results of the experimental data by the proposed electrical circuits (EC) are shown in Fig. 5 by real lines. It can be seen that the model results are significantly close to the experimental data.

Equivalent circuits proposed for fitting of EIS plots are given in the insert diagram according to various periods of corrosion process. Where $R_s$ is the electrolyte resistance; $Q_c$ is the constant phase element (CPE, denoted as $Q$ in the equivalent circuit) related to coating capacitance. The CPE is introduced instead of pure capacitance in the simulations to obtain good agreement between the simulated and experimental data. The CPE impedance can be defined as $Z_{CPE}=Y_0^{-1}\cdot(j\omega)^{-n}$ [60−62], where $Y_0$ is the CPE-constant; j is the imaginary unit ($j^2=-1$); $\omega$ is the angular frequency ($\omega=2\pi f$, $f$ is the frequency) and $n$ is the exponent of the constant phase element. The CPE depends on both the parameter $Y_0$ and the exponent $n$. Generally, $0<n<1$; when $n=1$, the CPE behaves like ideal capacitor corresponding to the conventional double layer capacitance; and when $n=0$, resistor is represented [61,63].

An electrical circuit (EC), $R_s(Q_c(R_{po}(Q_{dl}R_{ct}(R_LL))))$ [33,34] was used to fit the typical EIS data during the initial stage(in Fig. 5(a)), where the $R_{po}$ is the pore resistance due to penetration of electrolyte, and $Q_{dl}$ is attributed to the double layer capacitance in the vulnerable regions exposed to the bottom of electrolyte penetration paths. The charge transfer resistance $R_{ct}$, in parallel with $Q_{dl}$, is ascribed to the electrochemical reaction in the same region. The inductive element $L$ in series to $R_L$ refers to the inductance phenomenon caused by pitting corrosion. The initial corrosion stage is the pitting−dissolution−redeposition period, which is consistent with Period I of the $\varphi_{corr}(t)$ curves.

In the second stage, the coating behaves like EC (2) (in Fig. 5(b)) [64]. In the EC (2), $R_c$ represents contact resistances between the particles; $C_p$−$R_p$ is related to the activation corrosion of alloy particles in the coating; CPE assigned to the layer $Q_f$, in parallel to the film resistance $R_f$, is attributed to the behavior of corrosion films on the surface of alloy particle. Usually, the obvious changes in the shape of impedance curves (Nyquist, Bode-magnitude or phase angle plots) could be used as the judgment for variations of EC [64,65]. However, the shape changes of the impedance diagram are usually not clearly observed even after the long-time soaking in corrosion media, and shape variation does not necessarily mean EC must change [64]. As a consequence, to obtain more accurate simulation, the continuous simulations with different time should be carried out using several possible EC. Figure 5(c) shows the simulation of Nyquist plots to two possible EC. It can

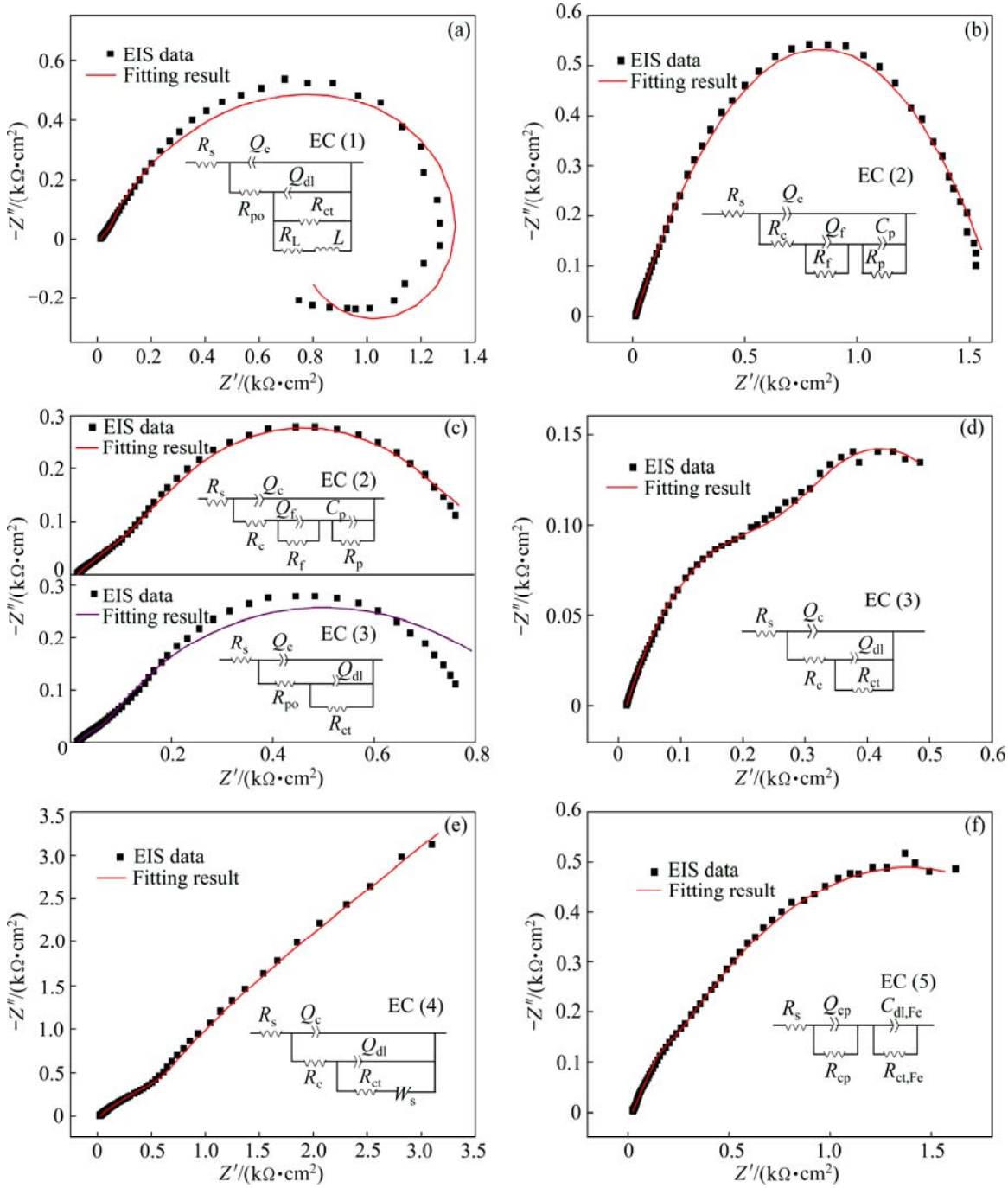


**Fig. 5** EIS plots and fitting results of Al−Zn−Si−RE coatings with different immersion time in 3.5% NaCl solution (Inserts display proposed equivalent circuits according to various periods of corrosion process: EC (1) pitting−dissolution−redeposition stage; EC (2) active dissolution stage; EC (3) cathodic protection stage; EC (4) physical barriers of corrosion products; and EC (5) coating failure stage): (a) 5 d; (b) 15 d; (c) 55 d; (d) 110 d; (e) 185 d; (f) 200 d

be seen that the experimental data in the third stage cannot be well fitted to the EC (3) while the EC (2) can give satisfactory simulation result. This result indicates that both the corrosion stages show similar corrosion behavior. Therefore, the two stages can be merged into one state called "activation corrosion period".

The typical EIS data obtained in the third stage is fitted to EC (3), as shown in Fig. 5(d). The equivalent circuit is composed of the solution resistance $R_s$, the pore resistance $R_{po}$ due to the formation of ion conducting paths across the coating, the coating capacitance $Q_c$, double-layer capacitance $Q_{dl}$ and charge transfer resistance $R_{ct}$. $Q_{dl}$ in parallel with $R_{ct}$ corresponds to electrochemical reaction at the coating/substrate interface, which reveals the initial attack to the substrate by the penetration of electrolyte [64]. It can be inferred that the

aggressive species have reached the substrate by diffusion through the small defects or pores in the coatings, resulting in galvanic corrosion between the alloy coating and the steel substrate. In this stage, the main protection mechanism of the coating/steel system is sacrificial anode cathodic protection.

The simulation and the corresponding EC (4), $R_s(Q_c(R_c(C_{dl}(R_{ct}W))))$ [55−66] of typical Nyquist plots obtained in the fourth stage are shown in Fig. 5(e). The diffusion resistance $W$ corresponding to the insulation of corrosion products occurs because the corrosion products cut off contact between the metal particles and the substrate [67]. Warburg impedance is usually also CPE which is defined by $W=[\sigma\omega]^{-\frac{1}{2}}(1-\mathrm{j})$ [68], where j is the imaginary number, $\sigma$ is the Warburg coefficient, $\omega=2\pi f$ is the angular frequency, and $f$ is the frequency. EC (4), $R_s(Q_c(R_c(C_{dl}(R_{ct}W))))$, is the so-called Randles circuit, which is used when the corrosion is controlled by diffusion process with diffusion of reactant and/or products to the interface [68]. Usually, the values of $\alpha$ in $W$ for different immersion time calculated from the EC (4) are deviated from the Warburg impedance, which is probably connected to "finite-layer diffusion" or the tangential penetration of electrolyte at the coating/substrate interface or by heterogeneous penetration of the electrolyte [48,64,69,70]. This corrosion stage is consistent with the Period IV in $\varphi_{corr}$−$t$ results.

The fitting results of EIS data after 200 d immersion and the corresponding EC (5) are shown in Fig. 5(f). EC (5) consists of the capacitance of corrosion products ($Q_{cp}$) in parallel to the resistance ($R_{cp}$ ) and the electric double layer capacitor on the steel surface ($C_{dl,Fe}$) in parallel to the resistance of corrosion reaction ($R_{ct,Fe}$).

Based on the analysis above, the electrochemical process occurring at the coating/electrolyte interface comprises five stages such as pitting-dissolution-redeposition on the coating surface, activation corrosion of alloy particles in the coating, cathodic protection after corrosion media reach the steel substrate, diffusion impedance responses caused by insoluble corrosion products and the impedance associated with coating failure and substrate corrosion.

## 5 Conclusions

1) Al−Zn−Si−RE coating shows very similar polarization behavior as Zn−15Al coating. The coating has no passive region in the anodic polarization region, but far lower corrosion current and much higher corrosion potential. Sacrificial anodic protection plays dominant role during immersion in 3.5% NaCl solution.

2) The $\varphi_{corr}$−$t$ curves and EIS results indicate that the corrosion process of Al−Zn−Si−RE coating in NaCl-containing environment has five distinct stages, i.e. pitting−dissolution−redeposition, activation corrosion, cathodic protection, physical barriers formed by corrosion products and the coating failure.

## References


[1] XIAO Yu-xing, JIANG Xin-hua, XIAO Yi-de, MA Liang-li. Research on Zn−Al15 thermal spray metal coating and its organic painting compo site system protection performance [J]. Procedia Eng, 2012, 27: 1644−1653.

[2] ORLANDO S, OLADIS T D R, ROJAS D, TOSAYA A, ROMERO N, SÁNCHEZ M, CAMPOS W. Six-year evaluation of thermal-sprayed coating of Zn/Al in tropical marine environments [J]. Int J Corros, 2012, 2012: 318279.

[3] CALLA E, MODI S C. Long life corrosion protection of steel by zinc aluminum coating formed by thermal spray process [J]. Trans Met Finishers Assoc India, 2001, 10: 21−26.

[4] KURODA S, KAWAKITA J, TAKEMOTO M. An 18-year exposure test of thermal-sprayed Zn, Al and Zn−Al coatings in marine environment [J]. Corrosion, 2006, 62(7): 635−647.

[5] ORLANDO S, OLADIS T D R, ÁLVARO R, MIGUEL S, MALDONADO L. Long-term performance of thermal sprayed coatings in tropical marine environments [C]//Proceedings of the International Corrosion Conference Series. Tennessee: NACE International, 2007.

[6] RANA R S, PUROHIT R, DAS S. Reviews on the influences of alloying elements on the Microstructure and mechanical properties of aluminum alloys and aluminum alloy composites [J]. Int J Sci Res Publ, 2012, 2(6): 1−7.

[7] LIU Kui-ren, MA Peng-cheng, PU Nian-wen, CHEN Jian-she, HAN Qing. Influence of silicon coating on the corrosion resistance of Zn−Al−Mg−RE−Si alloy [J]. J Rare Earths, 2010, 28(s1): 378−382.

[8] XIONG W, QI G T, GUO X P, LU Z L. Anodic dissolution of Al sacrificial anodes in NaCl solution containing Ce [J]. Corros Sci, 2011, 53(4): 1298−1303.

[9] AMADEH A, PAHLEVANI B, HESHMATI-MANESH S. Effects of rare earth metal addition on surface morphology and corrosion resistance of hot-dipped zinc coatings [J]. Corros Sci, 2002, 44(10): 2321−2331.

[10] GAO Hai-yan, TAN Juan, JU Chen, CHU Shuang-jie, WANG Jun, SUN Bao-de. Effect of rare earth metals on microstructure and corrosion resistance of Zn−0.18Al coatings [J]. Mater Sci Technol, 2011, 27(1): 71−75.

[11] LIU Yan, ZHU Zi-xin, MA Jie, XU Bin-shi, MA Shi-ning, LI Zhuo-xin. Effects of rare-earth metal on microstructure and corrosion resistance of arc-sprayed Zn−Al−Mg coating [C]//Proceedings of the ITSC 2005. Switzerland: ASM Thermal Spray Society, 2005: 1468−1472.

[12] LIU Yan, ZHU Zi-xin, CHEN Yong-xiong, XU Bin-shi, MA Shi-ning, LI Zhuo-xin. Electrochemical corrosion behavior of arc sprayed Zn−Al coatings [J]. Transactions of Nonferrous Metals Society of China, 2004, 14(S1): s443−s445.

[13] ZHU Zi-xin, XU Bin-shi, CHEN Yong-xiong. Effect of Al content on electrochemical corrosion behavior of arc sprayed Zn−Al coatings [J]. China Surf Eng, 2011(6): 58−61. (in Chinese)

[14] YANG Li-jing, ZHANG Yang-ming, ZENG Xu-duo, SONG Zhen-lun. Corrosion behavior of superplastic Zn−Al alloys in simulated acid rain [J]. Corros Sci, 2012, 59: 229−237.

[15] KAIN R M, BAKER E A. Marine atmospheric corrosion museum report on the performance of thermal spray coatings on steel [J]. Testing of Metallic and Inorganic Coatings, 1987, 974: 211−234.

[16] FENG Li-xin, ZHANG Min-yan, ZHANG Ping-ze. A multi-component zinc-aluminium alloy wire and its manufacturing methods: China, CN102703763 [P]. 2012−10−03. (in Chinese)

[17] LIU Yan, XU Bin-shi, ZHU Zi-xin, LIANG Xue-bing, CHEN Yong-xiong. Microstructure and corrosion behavior of arc sprayed Zn−Al−Mg−RE cathodic protection coatings on steel substrates [J]. Int Heat Treat Surf Eng, 2009, 3(1−2): 70−74.

[18] XU J, SUN C, YAN M C, WANG F H. Effects of sulfate reducing bacteria on corrosion of carbon steel Q235 in soil-extract solution [J]. Int J Electrochem Sci, 2012, 7(11): 11281−11296.

[19] BARRANCO V, FELIU S Jr, FELIU S. EIS study of the corrosion behaviour of zinc-based coatings on steel in quiescent 3% NaCl solution. Part 1: Directly Exposed Coatings [J]. Corros Sci, 2004, 46: 2203−2220.

[20] CHAUDHARI S, GAIKWAD A B, PATIL P P. Synthesis and corrosion protection aspects of poly(o-toluidine)/CdO nanoparticle composite coatings on mild steel [J]. J Coat Technol Res, 2010, 7(1): 119−129.

[21] DURAISAMY R, POWNSAMY K, ASGEDOM G. Chemical degradation of epoxy-polyamide primer by electrochemical impedance spectroscopy [J]. ISRN Corrosion, 2012, 2012: 819719.

[22] HE Xiao-dong, SHI Xian-ming. Self-repairing coating for corrosion protection of aluminum alloys [J]. Prog Org Coat, 2009, 65(1): 37−43.

[23] ZAND R Z, VERBEKEN K, ADRIAENS A. Electrochemical assessment of the self-healing properties of cerium doped sol−gel coatings on 304L stainless steel substrates [J]. Int J Electrochem Sci, 2012, 7(10): 9592−9608.

[24] YARO A S, HAMEED K W. Sacrificial anode cathodic protection of low carbon steel in seawater [J]. J Eng, 2007, 13(3): 780−1790.

[25] MA Jing-ling, WEN Jiu-ba, LI Geng-xin, XU Chun-hua. The corrosion behavior of Al−Zn−In−Mg−Ti alloy in NaCl solution [J]. Corros Sci, 2010, 52(2): 534−539.

[26] HE Jun-guang, WEN Jiu-ba, LI Xu-dong. Effects of precipitates on the electrochemical performance of Al sacrificial anode [J]. Corros Sci, 2011, 53(5): 1948−1953.

[27] WEN Jiu-ba, MA Jing-ling, HE Jun-guang. Al-base sacrificial anode material for corrosion protection [M]. Beijing: Chemical Industry Press, 2012: 67−79. (in Chinese)

[28] VENKATASUBRAMANIAN G, MIDEEN S, JHA A K. Effect of pH on the corrosion behavior of aluminum alloy welded plate in chloride solutions [J]. Res J Chem Sci, 2013, 3(6): 74−80.

[29] LIU Bing, LIU Lin. Effect of micro Mo addition on anticorrosion ability of Cu base bulk metallic glass [J]. Acta Metall Sinica, 2007, 43(1): 82−86. (in Chinese)

[30] PATEL N S, MENGHANI J, PAI K B, TOTLANI M K. Corrosion behavior of $Ti_2N$ thin films in various corrosive environments [J]. J Mater Environ Sci, 2010, 1(1): 34−43.

[31] GIL L E, LISCANO S, GOUDEAU P, BOURHIS E L, PUCHI-CABRERA E S, STAIA M H. Effect of TiAlN PVD coatings on corrosion performance of WC−6%Co [J]. Surf Eng, 2008, 26(8): 562−566.

[32] MORIMOTO Y, HONDA K, NISHIMURA K, TANAKA S, TAKAHASHI A, SHINDO H, KUROSAKI M. Excellent corrosion-resistant Zn−Al−Mg−Si alloy hot-dip galvanized steel sheet “SUPER DYMA” [J]. Shinnittetsu Giho, 2002, 87: 22−24.

[33] XIN Yun-chang, LIU Cheng-long, ZHANG Wen-jun, JIANG Jiang, TANG Guo-yi, TIAN Xiu-bo, CHU P K. Electrochemical behavior of $Al_2O_3$/Al coated surgical AZ91 magnesium alloy in simulated body fluids [J]. J Electrochem Soc, 2008, 155(5): 178−182.

[34] XIN Y C, JIANG J, HUO K F, TANG G Y, TIAN X B, CHU P K. Corrosion resistance and cytocompatibility of biodegradable surgical magnesium alloy coated with hydrogenated amorphous silicon [J]. J Biomed Mater Res A, 2009, 89(3): 717−726.

[35] MEROUFEL A, TOUZAIN S. EIS characterization of new zinc-rich powder coatings [J]. Prog Org Coat, 2007, 59(3): 197−205.

[36] HAMMOUDA N, CHADLI H, GUILLEMOT G, BELMOKRE K. The corrosion protection behavior of zinc rich epoxy paint in 3% NaCl solution [J]. Adv Chem Eng Sci, 2011, 1(2): 51−60.

[37] ABREU C M, IZQUIERDO M, KEDDAM M, NOVOA X R, TAKENOUTI H. Electrochemical behavior of zinc-rich epoxy paints in 3% NaCl solution [J]. Electrochim Acta, 1996, 41(15): 2405−2415.

[38] HU Hui-li, LI Ning, CHENG Jin-ning, CHEN Li-jiao. Corrosion behavior of chromium-free dacromet coating in seawater [J]. J Alloys Compd, 2009, 472(1): 219−224.

[39] OSTANINA T N, RUDOIV M, YAROSLAVTSEVA O V, SOLOV’EV A S, SUBBOTINA O Y, DOKASHENKO S I. Protective properties of zinc-rich coatings: An impedance method estimate [J]. Russ J Electrochem, 2004, 40(10): 1019−1023.

[40] ZHANG Y J, YAN C W, WANG F H, LI W F. Electrochemical behavior of anodized Mg alloy AZ91D in chloride containing aqueous solution [J]. Corros Sci, 2005, 47: 2816−2831.

[41] ZHOU Wen-juan, XU Li-kun, WANG Jia, LI Ning, XUE Li-li, CHEN Guang-zhang. Corrosion electrochemical behavior of Zn−Al silane coating on carbon steel [J]. Acta Metall Sinica, 2007, 43(9): 983−988. (in Chinese)

[42] SINGH A K, QURAISHI M A. Effect of cafazolin on the corrosion of mild steel in HCl solution [J]. Corros Sci, 2010, 52: 152−160.

[43] PARDO A, MERINO M C, COY A E, VIEJO F, ARRABAL R, FELIÚ J S. Influence of microstructure and composition on the corrosion behavior of Mg/Al alloys in chloride media [J]. Electrochim Acta, 2008, 53(27): 7890−7902.

[44] FRANKEL G S. Pitting corrosion [M]//CRAMER S D, COVINO B S Jr. ASM Handbook. Vol. 13A: Corrosion: Fundamentals, Testing, and Protection. OH: ASM International, 2003: 236−241.

[45] GHODS P, ISGOR O B, MCRAE G A, LI J, GU G P. Microscopic investigation of mill scale and its proposed effect on the variability of chloride-induced depassivation of carbon steel rebar [J]. Corros Sci, 2011, 53(3): 946−954.

[46] LEBRINI M, ROBERT F, ROOS C. Adsorption properties and inhibition of C38 steel corrosion in hydrochloric solution by some indole derivates: Temperature effect, activation energies, and thermodynamics of adsorption [J]. Int J Corros, 2013, 2013: 139798.

[47] GOUVEIA-CARIDADE C, PEREIRA M I S, BRETT C M A. Electrochemical noise and impedance study of aluminum in weakly acid chloride solution [J]. Electrochim Acta, 2004, 49(5): 785−793.

[48] SALMAN S A, ICHINO R, OKIDO M. A comparative electrochemical study of AZ31 and AZ91 magnesium alloy [J]. Int J Corros, 2010, 2010: 412129.

[49] ISHIZAKI T, MASUDA Y, TESHIMA K. Composite film formed on magnesium alloy AZ31 by chemical conversion from molybdate/phosphate/fluorinate aqueous solution toward corrosion protection [J]. Surf Coat Technol, 2013, 217: 76−83.

[50] LIANG Ping, ZHANG Yun-xia, HU Chuan-shun. Effect of corrosion products films on corrosion behavior of X80 pipeline steel in Ku’erle soil simulated solution [J]. J Mater Eng, 2012, 12(4): 62−67. (in Chinese)

[51] ZHANG J T, HU J M, ZHANG J Q, CAO C N. Studies of impedance models and water transport behaviors of polypropylene coated metals in NaCl solution [J]. Prog Org Coat, 2004, 49(4): 293−301.

[52] RODRÍGUEZ-DIAZ R A, URUCHURTU-CHAVARÍ J, MOLINA-OCAMPO A, PORCAYO-CALDERON J, MENDOZA M E,

VALDEZ S, JUÁREZ-ISLAS J. Hot corrosion behavior of FeAl intermetallic compound modified with silver in molten salt mixture [J]. Int J Electrochem Sci, 2013, 8: 11877−11895.

[53] DURAISAMY R, POWNSAMY K, ASGEDOM G. Chemical degradation of epoxy-polyamide primer by electrochemical impedance spectroscopy [J]. ISRN Corrosion, 2012, 2012: 819719.

[54] SHI H W, LIU F H, HAN E H, WEI Y H. Effects of nano pigments on the corrosion resistance of alkyd coating [J]. J Mater Sci Technol, 2007, 23(4): 551−558.

[55] BARSOUKOV E, MACDONALD J R. Impedance sprectroscopy theory, experiment, and applications [M]. New York: Wiley-Interscience, 2005.

[56] MARCHEBOIS H, TOUZAIN S, JOIRET S, BERNARD J, SAVAL C. Zinc-rich powder coatings corrosion in sea water: Influence of conductive pigments [J]. Prog Org Coat, 2002, 45(4): 415−421.

[57] MARCHEBOIS H, SAVALL C, BERNARD J, TOUZAIN S. Electrochemical behavior of zinc-rich powder coatings in artificial sea water [J]. Electrochim. Acta, 2004, 49(17): 2945−2954.

[58] XU A T, ZHANG F, LUO B, JIN F, ZHANG T R. Investigation the protective performance of organic coatings with different breakage degree busing EIS united to SOM neural network [J]. Int J Electrochem Sci, 2013, 8: 1895−1902.

[59] ZHANG J F, ZHANG W, YAN C W, DU K Q, WANG F H. Corrosion behaviors of Zn/Al−Mn alloy composite coatings deposited on magnesium alloy AZ31B (Mg−Al−Zn) [J]. Electrochim Acta, 2009, 55(2): 560−571.

[60] SOUTO R M, FERNÁNDEZ-MÉRIDA L, GONZÁLEZ S, SCANTLEBURY D J. Comparative EIS study of different Zn-based intermediate metallic layers in coil-coated steels [J]. Corros Sci, 2006, 48(5): 1182−1192.

[61] MARECI D, CHELARIU R, SUTIMAN D, RUSU I. Electrochemical characteristics of electrochemically patinated bronze [J]. Eur J Sci Theology, 2011, 7(4): 121−129.

[62] BOLAT G, MARECI D, IACOBAN S, CIMPOESU N, MUNTEANU C. The estimation of corrosion behavior of NiTi and NiTiNb alloys using dynamic electrochemical impedance spectroscopy [J]. J Spectro, 2013, 2013: 714920.

[63] ZHOU Q X, WANG Y C, BIERWAGEN G P. Influence of the composition of working fluids on flow-accelerated organic coating degradation: Deionized water versus electrolyte solution [J]. Corros Sci, 2012, 55: 97−106.

[64] HU J M, ZHANG J Q, CAO C N. Determination of water uptake and diffusion of $Cl^-$ ion in epoxy primer on aluminum alloys in NaCl solution by electrochemical impedance spectroscopy [J]. Prog Org Coat, 2003, 46(4): 273−279.

[65] WEI D F, CHATTERJEE I, JONES D A. Evaluation of corrosive degradation in coated steel using alternating current impedance spectroscopy [J]. Corrosion, 1995, 51(2): 97−104.

[66] LIU J G, YAN C W. Electrochemical characteristics of corrosion behavior of organic/Dacromet composite systems pretreated with gamma-aminopropyltriethoxysilane [J]. Surf Coat Technol, 2006, 200(16): 4976−4986.

[67] CHEN L, LI N, ZHOU D R. Corrosion behavior of sintered zinc−aluminum coating in NaCl solution [J]. Transactions of Nonferrous Metals Society of China, 2002, 12(6): 1214−1217.

[68] DURAISAMY R, POWNSAMY K, ASGEDOM G. Chemical degradation of epoxy-polyamide primer by electrochemical impedance spectroscopy [J]. ISRN Corrosion, 2012, 2012: 819719.

[69] GUO X H, DU K Q, GUO Q Z, WANG Y, WANG F H. Experimental study of corrosion protection of a three-layer film on AZ31B Mg alloy [J]. Corros Sci, 2012, 65: 367−375.

[70] ZHU C F, XIE R, XUE J H, SONG L L. Studies of the impedance models and water transport behaviors of cathodically polarized coating [J]. Electrochim Acta, 2011, 56(16): 5828−5835.

# 电弧喷涂 Al−Zn−Si−RE 合金涂层在 3.5%NaCl 溶液中的电化学腐蚀行为

蒋 穹，缪 强，仝 飞，徐 一，任蓓蕾，刘志梅，姚正军

南京航空航天大学 材料科学与技术学院，南京 211100

**摘 要**：采用电弧喷涂方法在低碳钢表面获得高铝含量的 Al−Zn−Si−RE 涂层。通过测量 Al−Zn−Si−RE 涂层在 3.5%NaCl 溶液中的动电位极化曲线，腐蚀电位−时间曲线和电化学阻抗谱，系统地研究涂层的电化学腐蚀行为。通过将测量电化学阻抗谱拟合成等效电路图，研究涂层在 3.5%NaCl 溶液中浸泡不同时间的阻抗行为。结果表明：Al−Zn−Si−RE 涂层与 Zn−15Al 涂层具有相似的极化行为，阳极极化曲线均无钝化特征，仅呈现出活性溶解，但其腐蚀性能优于 Zn−15Al 涂层。Al−Zn−Si−RE 涂层可以给钢基体提供有效的牺牲阳极保护作用，且牺牲阳极保护作用在涂层腐蚀过程中占主导地位。此外，腐蚀电位−时间曲线和电化学阻抗谱结果表明：在浸泡过程中存在点蚀−溶解−再沉积、活化溶解、阴极保护、腐蚀产物引起的物理屏蔽和涂层失效五个腐蚀阶段。

**关键词**：Al−Zn−Si−RE 涂层；腐蚀电位；腐蚀行为；极化曲线；电化学阻抗谱

**(Edited by Chao WANG)**